A NANOSECOND UV LIGHT SOURCE FOR MONITORING AND CALIBRATING WATER CERENKOV COUNTERS

Harold Lessure

Honors Thesis in Physics
January 1983

Randall Laboratory
University of Michigan
Ann Arbor, MI 48109

Advisor: Dr. L.R. Sulak

TABLE OF CONTENTS

A NANOSECOND UV LIGHT SOURCE FOR MONITORING AND CALIBRATING WATER CERENKOV COUNTERS

ABSTRACT:

The characteristics of a water Cerenkov monitoring and calibrating system are described. A nitrogen laser provides nanosecond pulses of ultraviolet light. The time of firing and the pulse height of the light pulses are under computer control. The laser light is guided to the detectors by an optical fiber. At the end of the fiber the light pulse may be isotropically dispersed to light thousands of PMTs viewing the same water volume. The time resolution of PMTs as well as pulse height response and resolution (from the single photoelectron level to phototube saturation) are measured using a single fast photomultiplier tube and a 128 PMT array in air. This system will also be of use in calibrating liquid scintillator detectors.

1. INTRODUCTION

Photomultiplier tubes (PMTs) are widely used as detectors of Cerenkov radiation because of their excellent time and energy resolution, and their sensitivity down to the single photoelectron level. Large arrays of PMTs (up to thousands of tubes) are being designed and constructed to detect the products of proton decay in water. The light system described here was developed to monitor and calibrate the Irvine-Michigan-Brookhaven (IMB) water Cerenkov detector. That detector consists of an array of 2048 PMTs evenly distributed over the faces of a cube of water 21 meters on a side.[1] Continuous monitoring of the detector with calibration flashes interspersed randomly during data taking can provide indispensible information on the performance of the detector. It is desirable in such a detector to mimic the sought for signal by firing all of the tubes at once with a single light pulse in the middle of the water volume. A centrally located source with an isotropic output is necessary. We have developed such a source producing pulses at each tube of varying intensity from fractions of a percent firing probability to hundreds of photoelectrons. Timing and intensity are under computer control.

In this paper we will describe the system elements and performance using both a single fast PMT and a large scale 128 PMT array in air with which the light source was perfected before installation in the water detector.

2. SYSTEM ELEMENTS

The block diagrams in Figures 1 and 2 give an overview of the system. Figure 1 details the components. The system operates in the following manner: A computer encodes firing time and pulseheight information into control signals for the laser and the optical processor, respectively. The nitrogen laser (chosen for its subnanosecond pulse length and 337 nm wavelength in the Cerenkov spectrum) is triggered. The beam firing is monitored by a photodiode and attenuated. Finally, an optical fiber transmission line conducts the light to an isotropic diffuser, which distributes the light to the PMTs.

Figure 2 shows detail of the optical processing section of Figure 1. A quartz window reflects a portion of the incident beam to the photodiode. A stepping motor selects a filter for the desired attenuation of the remainder of the beam. A positioning clamp is used to center the optical fiber in the filtered beam for best coupling.

CAMAC control signals determine the timing of the pulses and their attenuation in processing. The photodiode response, digitized by a time digitizer (TDC) and an analog to digital converter (ADC), gives information on the unfiltered beam. The beam transmission line is a fused silica optical fiber. It terminates in a spherical borosilicate cavity filled with a diffusing suspension. There, Rayleigh scattering produces an isotropic source.

An isolation transformer prevents high frequency transients from the laser spark gap trigger from entering the common AC. Gas regulation sets the spark gap sensitivity and maintains the proper flow of nitrogen in the lasing channel. Uniform channel flow insures that ions are evacuated so a reproducible light output results.

2.1 The Light Source

The nitrogen laser[2] was chosen for its wavelength, pulselength and triggerability. It provides enough energy to illuminate thousands of PMTs to saturation with the arrangement shown in Figure 1.

The wavelength of its output at 337 nm is between the lower half power point and the peak of the Cerenkov spectrum for a $\beta = 1$ singly charged particle as viewed through 10 m of water (see Figure 3c). This is the most vulnerable region of the spectrum because of the falloff of the primary spectrum in figure 3a and the transmission length of the water at 337 nm in figure 3b. Figure 3d shows the photocathode response of a typical bialkali photomultiplier[3] used as the primary detector element in the IMB experiment. The spectral response of bialkali PMTs is well matched to the ultraviolet radiation from Cerenkov light through water (cf. figures 3c and 3d).

The laser light pulses are short with respect to the 5 nanosecond transit time jitter of the PMT. Since the uncertainty in the timing of the laser output can be made very small (< 1.5 ns), the time resolution of the PMT dominates time fluctuation in PMT signals. Each pulse then yields a direct measurement of the time resolution of the PMT.

The laser is triggered by a sequence of two TTL level trigger pulses. A custom CAMAC unit[4] produces the timing signals with a dynamic range of 1 to 50 μs between pulses and with an accuracy of 0.5 ns.

We calibrate PMT response over a wide dynamic range of incident light levels from the 0.1 photoelectron level (10% firing probability) up to the highest light levels in the experiment i.e. 1000 photons per PMT at 10 meters from the diffuser ball. This requires the laser to produce a minimum of $\sim 10^{10}$ photons per pulse. The unfiltered direct beam has $\sim 10^{14}$ photons per pulse.

Additions and modifications have been made to the commercially obtained laser to ease maintenance and improve reliability. Important changes include external gas regulation, AC line current control, and HF noise suppression. Gas flow is controlled by a needle valve and monitored by a pressure gauge and flow meter. The power line has a ferrite core for noise suppression. The paint on laser housing mating surfaces has been removed to provide a conductive radiation tight seal.

2.2 Optical Processing

Beam manipulation to monitor and attenuate the laser output and couple it to the optical fiber is detailed in figure 2. The beam sampler is a thin, optically flat quartz plate which gives a 4% reflection at each face. The 8% removed from both faces is incident on the photodiode. The silicon photodiode was selected for its fast response (< 1 ns) and UV sensitivity[5]. It was necessary to make the leads in the photodiode circuit as short as possible to minimize high frequency pickup from the laser spark gap. The photodiode is used to measure fluctuations in the amplitude and timing of the laser output as well as to monitor laser efficiency.

The central beam continues to the filtering section which contains a filter wheel. The filter wheel contains filters[6] in five optical density steps at 337 nm which give a dynamic range of 600 in light filtering.[7] The durability of the filters is such that their optical densities should remain stable with prolonged exposure (> 5 years) to laser pulses at our pulse rates and intensities[8]. A sixth filter slot is left open as a 100% transmission reference. The filter wheel is used to step the intensity of the beam from the single photoelectron level to phototube saturation. A potentiometer readback and mechanical stop are used to set and verify the wheel position.

2.3 The Optical Fiber

Important parameters of the optical fiber are bandwidth and attenuation. The pulse dispersion in time is determined from the bandwidth by the formula[9]:

$$t_s = \frac{.318}{BW} \cdot \ell$$

where t_s is the FWHM spreading in seconds

BW is the bandwidth in Hz

ℓ is the fiber length in km.

For example, for this system, with ℓ = 45m and BW = 20 MHz/km, t_s = 0.72 ns. Since typical laser pulses are 0.5 ns FWHM the pulse broadening in the fiber is comparable to the time resolution of the photon pulses. The combined width of ~ 1 ns is significantly less than the timing jitter of the PMTs we are monitoring.

Although most optical fibers attenuate severly in the UV, we have found one that has a tolerable absorption and excellent mechanical durability. It is a fused silica teflon clad fiber[10]. The 300 μm fiber has a bandwidth of 20 MHz/km and a loss at 337 nm of -2.5 dB/m. For a 45 m length this is a loss of a factor of 4×10^5 in light intensity. The fiber has a numerical aperture of 0.26 corresponding to an acceptance angle of 15 degrees. The fiber comes with or without a protective jacket[11]. The cabled fibers resist a continuous tension of 42 lbs. and a transverse pressure of 250 lbs. when applied by two 2" metal plates.

2.4 Light Distribution

A method of diffusing the light is necessary to illuminate all the PMTs at the same time and to suppress fiber end modal patterns[12]. An effective means utilizes a suspension of small particles at the end of the fiber to isotropically scatter the light.

Two different scattering colloids have been successfully employed, a colloidal silica[13] and a polystyrene suspension[14]. These suspensions are commercially available, stable for years (not chemically delicate), and they contain uniform spherical particles with narrow size distributions.

Operation in the Rayleigh region where individual scatterings are nearly isotropic requires that[15]:

$$\frac{a}{\lambda} \leq 0.05 \quad (1)$$

where a is the particle radius

and λ is the wavelength of incident radiation.

For the colloidal silica $\frac{a_{silica}}{\lambda} = 0.031$

and for the polystyrene particles $\frac{a_{polystyrene}}{\lambda} = 0.126.$

These are the only commercially available, stable, uniform, particulate suspensions which we have found that approximate the a/λ criteria stated in (1) above. The polystyrene suspension should be expected to deviate from isotropy for single scatterings. However, both suspensions were found to produce nearly isotropic sources when there was sufficient multiple scattering. The anisotropy of a single scattering does not dominate the radiation pattern of the diffuser if we adjust the fiber output point position such that there is a relatively longer photon path length in the forward direction (cf. Figure 8b). Multiple scattering is calculated from the extinction equation[16]:

$$T = \exp\left[-N\ell\, C_{sca}\right].$$

T gives the transmission at a distance ℓ for photons passing through a suspension of N particles per unit volume whose cross sections are given by C_{sca}:[17]

$$C_{sca} = \frac{24\pi^3 V^4}{\lambda^4} \cdot \frac{n^2-1}{n^2+1}$$

where V is the particle volume,

λ is the wavelength of incident radiation,

and n is the relative index of refraction,

$$n = \frac{n\ (\text{particles})}{n\ (\text{medium})}\ .$$

3. PERFORMANCE

3.1 Evaluation with a Fast Photomultiplier Tube

The performance of the calibration system was evaluated with a five-inch fast response PMT[18] viewing the diffuser which could be oriented arbitrarily relative to the PMT. A LSI-11 microcomputer[19] was programmed to choose the desired attenuation filter, fire the laser, and collect the time and pulse height information from the PMT signal.

Standard operating conditions were set at a spark gap pressure of 12 psi, high voltage on the lasing channel of 16 kv, channel nitrogen flow of 20 cm^3/min, and channel pressure of 0.04 inches of water. The standard triggering rate was 20 pulses/sec. These operating conditions are stable and give reproducible results. Fine tuning of the spark gap spacing and pressure was required after approximately 10^6 pulses to maintain the lowest jitter in laser firing time relative to the trigger time.

3.1.1 Laser Efficiency

We examined the efficiency of the laser under various conditions of nitrogen pressure, high voltage, and triggering rate. The inefficiency was measured by the number of times a laser trigger was generated, but no pulse appeared at the photodiode or PMT. The mean inefficiency is 0.23% averaged daily over a period of 10 weeks, at the standard conditions described above. We found equally good results for repetition rates less than 20 Hz, but at higher repetition rates, the inefficiency increased to $\sim$ 10% at 50 Hz.

3.1.2 Timing Resolution

The time resolution is characterized by the jitter in the time between a request for a laser pulse and the resulting pulse at the PMT. Figure 4 shows a histogram of TDC values for 5000 requests. The TDC[20] was started by the trigger pulse to the laser and was stopped by the PMT output firing a 50 mV discriminator with a PMT output of 1.3V ± 0.3V. The standard deviation for the distribution in figure 4 is 1.5 ns. The time jitter was one to two nanoseconds under typical laser operating conditions[21] over a period of six months.

The critical timing measurement was the time jitter between the photodiode response and the PMT response since this eliminates time variations in the laser. The TDC histogram which shows events whose starting times were at the photodiode discriminated output are shown in figure 5. Five thousand events are displayed >90% of which fall in two adjacent bins (.8ns). These variations are directly attributed to the PMT jitter.

3.1.3 Amplitude Response

We measured the amplitude fluctuations of the system by making a histogram of the charge output[22] measured by the PMT. The histogram is reproduced in figure 6 below. Letting $\langle Q \rangle$ be the mean charge deposition we measure the ratio $\sigma/\langle Q \rangle$ to be 9% pulse to pulse. These 9% variations agree with the photodiode pulse height variations.

3.1.4 Fiber Attenuation Measurements

Attenuation of the beam due to the optical fiber arise both at the beam-fiber interface and through the length of the fiber. Coupling losses are due to the acceptance angle of the fiber and fiber end reflections. The absorption and scattering arise from impurities in the core fiber and at the core/sheath internal reflection interface.[23] Losses depend strongly on wavelength. Since no published data is available for our fiber at 337 nm we measured the attenuation. Figure 7 shows the results. The graphs show an attenuation of -2.5 dB/m (a factor of 10 decrease per 8 m). This gives an attenuation length of 3.5 m. The upper curve shows an overall factor 2.5 higher level of light due to a flat cleaved input end relative to the other fiber. We find that this factor represents the typical range in acceptance between fibers cleaved randomly. Cleaved fiber ends are microscopically inspected for surface imperfections.

3.1.5 Light Scattering

A graph of the angular distribution of a typical diffuser is given in figure 8a. The light is isotropic to ± 20%. The direction of maximum light output is dependent on where the fiber terminated in the ball (cf. fig 8b). Figure 8a shows an instance where fiber end location favors light scattering in the forward ($\Theta = 0^{\circ}$) direction. The geometry used for the figure 8a radiation pattern was a 1.5 cm diameter quartz sphere filled with a 1:84 dilution of the polystyrene solution in water. The fiber end was centered in the sphere by eye.

3.2 Large Scale Tests

A surface array of 128 PMTs on a 4 m cube was arranged in a light tight room at the University of Michigan. The photomultipliers used in the array were EMI 9870B PMTs destined for use in the IMB proton decay detector. The PMTs were arranged along the walls of the room at regular intervals with 32 PMTs per wall. There were no PMTs on the ceiling or floor. The laser diffuser ball was centered in the room. The electronic readout of the 128 PMT array was similar to the readout of the single PMT test setup. A calibration curve of the mean charge output of the tubes vs. relative light intensity is plotted in figure 9. The curve shows an approximately logarithmic response at high light levels where the tubes begin to saturate. This curve may be put on an absolute scale by using Poisson statistics to determine the average number of photons per tube at low light levels. This is accomplished by choosing a light filter for which the average probability of firing the PMT is $\sim 10\%$, thus assuming single photon operation. The average number of photoelectrons is given by $\langle n \rangle$.

$$\langle n \rangle = -\ell n\,(1-occ)$$

where occ = occupancy i.e. the percentage of times the PMT exhibits response.

With a knowledge of $\langle n \rangle$, the number of photons observed at high light levels may be found by scaling $\langle n \rangle$ according to the transmission of the known filter chosen in the system. Using the light system described in this paper, the 128 PMTs are calibrated in time and in pulse height from 10% occupancy to 100 photoelectrons per tube satisfactorily over a period of three months.

4. SUMMARY

A light pulse system has been developed which produces UV light useful for the calibration of PMTs viewing Cerenkov radiation.[24] The pulse width is $\sim$ 1 ns and jitter with respect to the photodiode is less than 1 ns. Pulse intensities are varied between the single photoelectron level and levels high enough to saturate 5 inch PMTs 10 m in water from the source. The output is conveniently handled and directed by using a fused silica optical fiber. The fiber output is isotropically dispersed using Rayleigh scattering.

The system can be used to test and calibrate single PMTs or large arrays. Currently a second generation of the apparatus is monitoring and calibrating the 2048 PMT Irvine-Michigan-Brookhaven proton decay detector.

ACKNOWLEDGEMENTS

The author would like to express thanks to the several members of the IMB collaboration who contributed to the development of the system described here. In particular Richard Bionta, Bruce Cortez, Bill Foster, Eric Shumard, and Jim Stone deserve credit. Special recognition is due to the physicists at the University of Michigan specializing in non-linear optics, John Dudley, Dan Elliot*, Mike Myers**, and John Ward. K. Rao had a major role in design and construction of optical components and laser modifications. Our gratitude is extended as well to many others with whom we consulted, including Jim Strait of Lawrence Berkeley Lab and John Box of Photochemical Research Associates.

I am particularly grateful to my research advisor Dr. Lawrence Sulak whose patience and recommendations enabled me to pursue this research. This work has been supported in part by the United States Department of Energy.

* Max Planck Institute, München, Germany

** Shell Development Co., Houston, TX

REFERENCES

1. A description of the IMB detector is given by: L.R. Sulak, in First Workshop on Grand Unification, Univ. of New Hampshire, April 1980.
2. PRA LN103 nitrogen laser; Photochemical Research Associates Inc., London, Ontario, Canada.
3. EMI 9870B 5" hemispherical phototube; Thorn EMI Gencom Inc., Plainview, N.Y.
4. Custom CAMAC laser controller designed by W. Foster of the IMB collaboration.
5. MRD500 silicon photodiode, Motorola Semiconductor Data Library Vol. 3, 1974, p. 1259; This photodiode recommended by J. Box of Photochemical Research Associates, private communication.
6. Neutral density filters on quartz substrates by Melles Griot, Irvine, CA.
7. Melles Griot filter attenuation curves give percent transmission values of 18%, 3.0%, 1.1%, 0.36%, and 0.15% for our five filters rounded to two significant figures at 337 nm.
8. Melles Griot neutral density energy/power dissipation via K. Rao, private communication.
9. Bandwidth and (risetime-bandwidth) product for our fiber from Rudy Montgelas, Belden Corp. engineering, Geneva, Il, private communication.
10. QSF series fused silica optical fibers, Quartz Products Corp., Plainsfield, N.J.
11. Protective cabling provided by Belden Corp., Geneva, Il. Figures quoted on cabled fiber durability by Rudy Montgelas, Belden Corp., private communication.
12. N.S. Kapany, Fiber Optics, Principles and Applications, London New York . Academic Press, 1967, p. 58.

13. Ludox TM colliodal silica manufactured by Dupont Chemical Corp., Wilmington, DE.

14. Spherical polystyrene particle suspension from Dow Chemical Co., Indianapolis, IN.

15. M. Kerker, The Scattering of Light and Other Electromagnetic Radiation, New York Academic Press, 1969, p. 324.

16. M. Kerker, Ibid., p. 37.

17. M. Kerker, Ibid., p. 85.

18. R1250 phototube; Hamamatsu Corp., Middlesex, N.J.

19. LSI-11 and PDP 11-34 computers are products of Digital Corp., Maynard, MA.

20. TDC model TD104 manufactured by EG&G, Oak Ridge, TN.

21. Typical laser operating parameters are quoted in Section 3.1 of this text (see standard conditions ... p.8). Adjustment of the spark gap trigger was necessary as noted to maintain fastest laser response to trigger input pulses.

22. PMT charge output integrated using charge digitizer (QDC) model QC808 from EG&G, Oak Ridge, TN.

23. W.B. Allan, Fiber Optics, Theory and Practice, London New York Plenum Press, 1973, pp. 47-49, 199.

24. A revised and extended version of this paper will be submitted to Nuclear Instruments and Methods.

FIGURE CAPTIONS

Figure 1. Block diagram of entire laser system showing major elements and electronic control.

Figure 2. Diagrammatic enlargement of optical processor with detail of beam monitoring and manipulation.

Figure 3. a,b,c,d. Spectra comparing Cerenkov light production and attenuation for $\beta=1$ singly charged particle in water with bialkali photocathode response.

Figure 4. Histogram of digitized times between laser pulse request and discriminated PMT output for 5000 laser requests.

Figure 5. Histogram of digitized times between discriminated photodiode output and discriminated PMT output for 5000 laser requests.

Figure 6. Histogram of integrated PMT output charge exhibiting the variations in laser energy output for 5000 events.

Figure 7. Attenuation curve at 337 nm for two fused silica optical fibers with different fiber input face qualities.

Figure 8a. Rayleigh diffuser far field radiation pattern for a fiber whose end is centered in the diffuser sphere. Line hand drawn to guide the eye.

Figure 8b. Fiber end placement in Rayleigh diffuser.

Figure 9. Calibration curve of integrated phototube output charge as a function of beam energy.

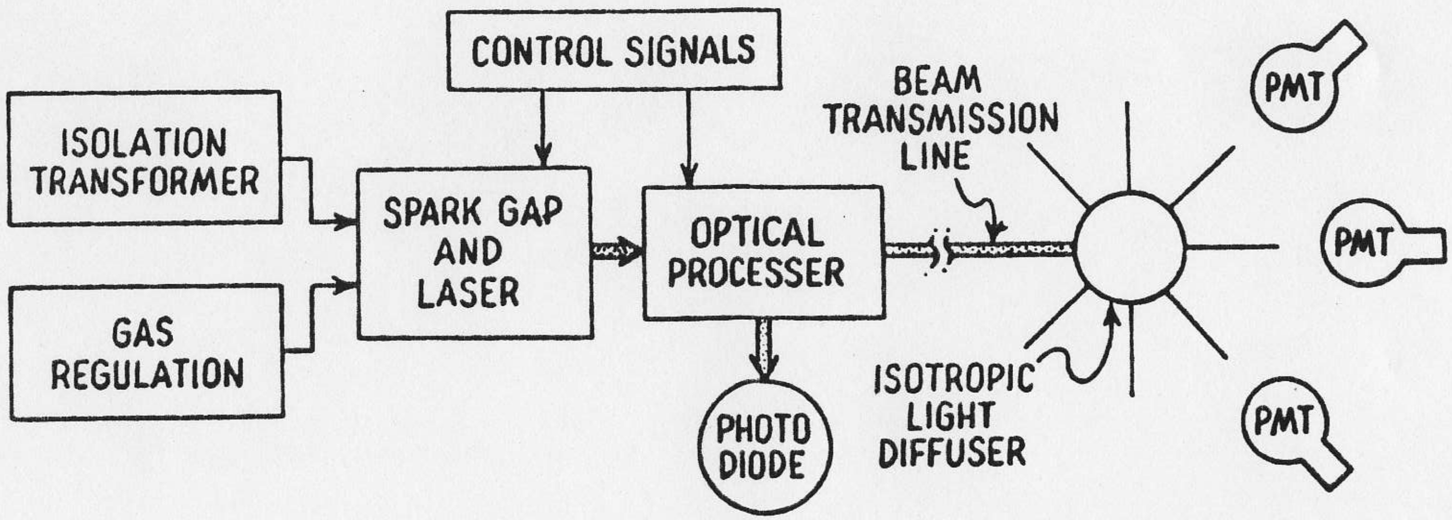

Figure 1. Laser Light System Block Diagram

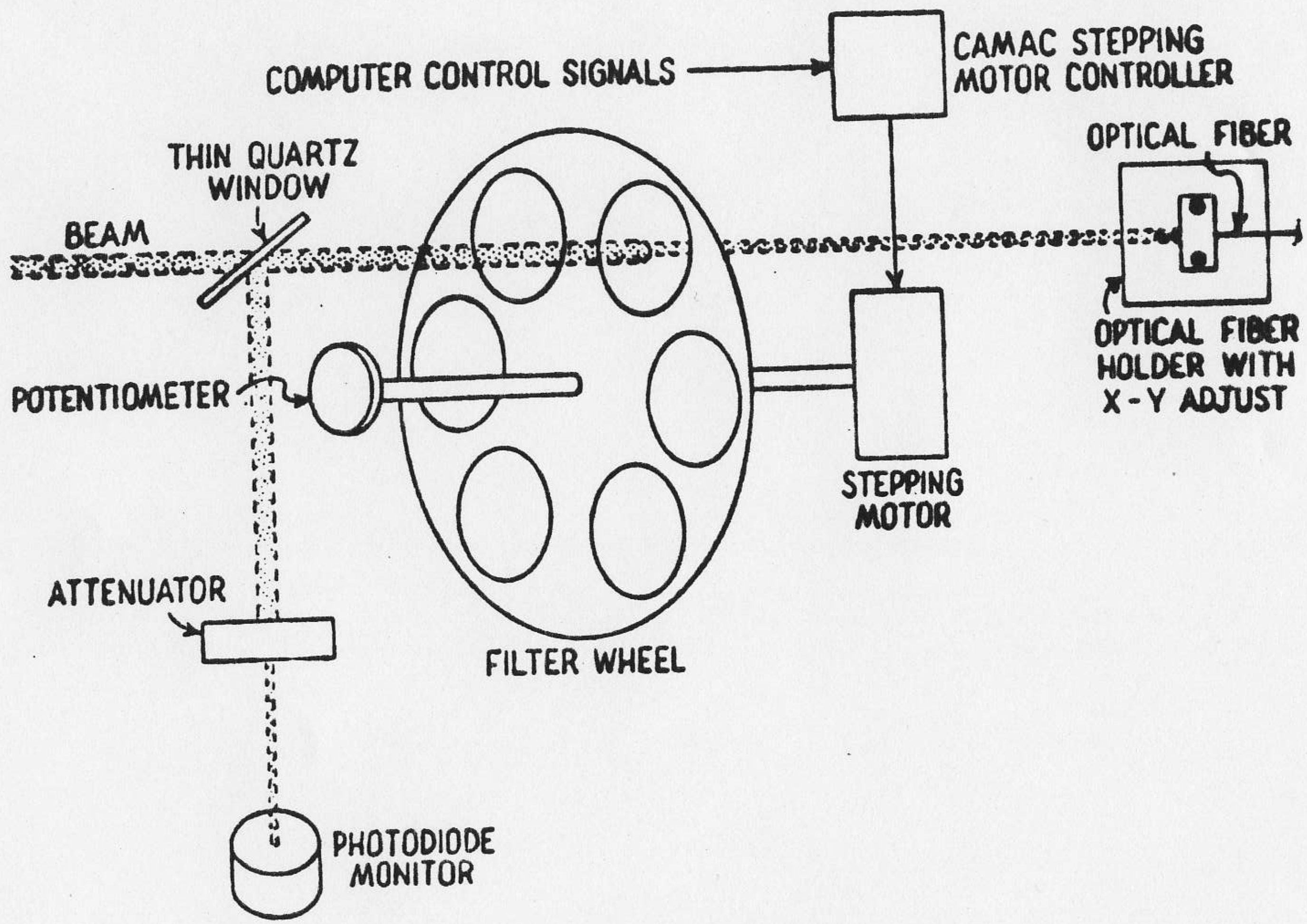

Figure 2. Detail of Optical Processer

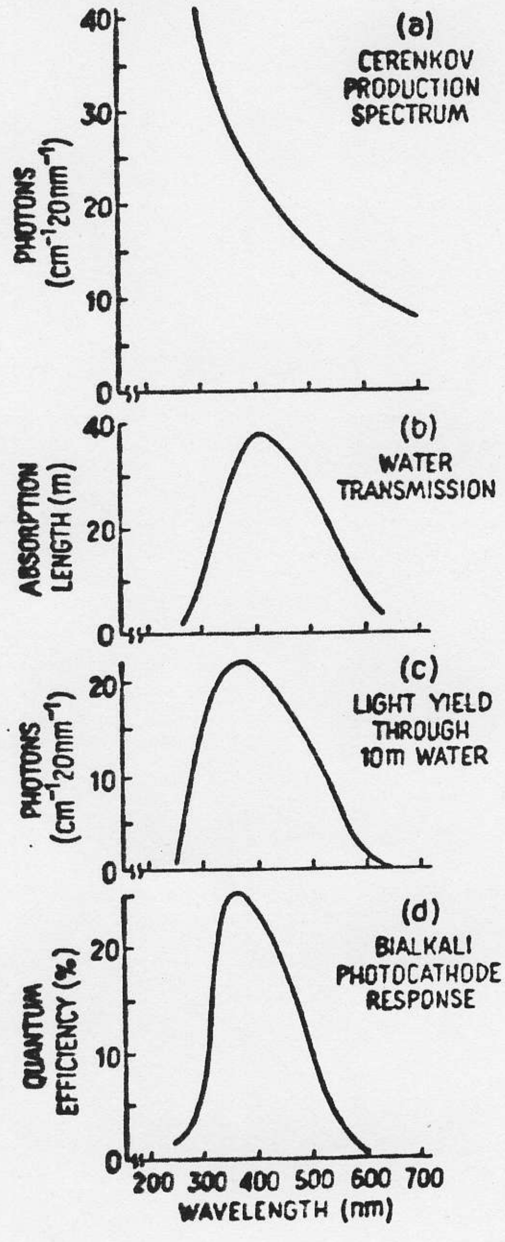

Figure 3. Cerenkov Light Production, Water Attenuation, and Bialkali Photocathode Response

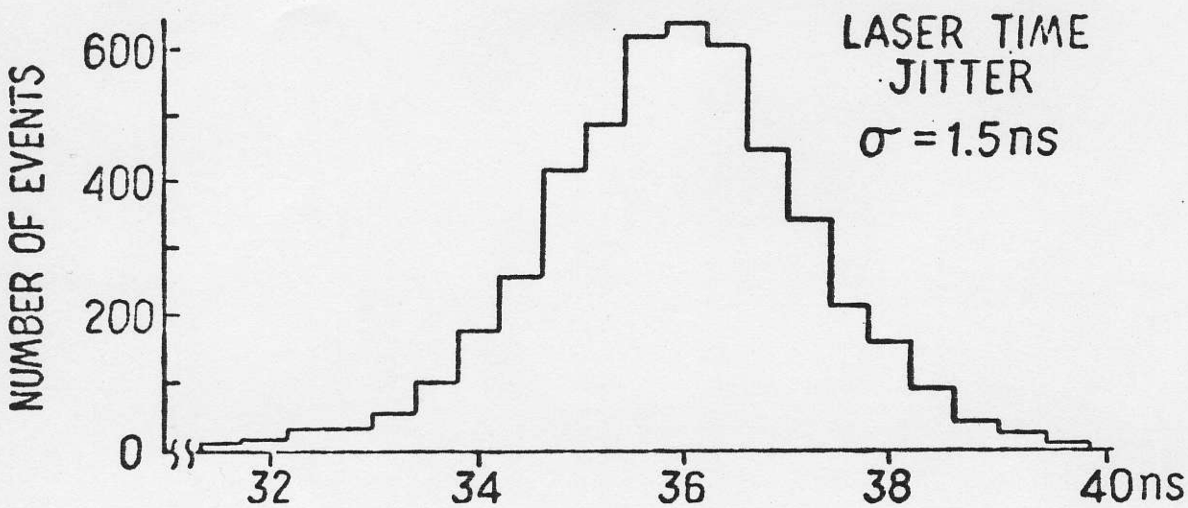

Figure 4. Laser Time Response

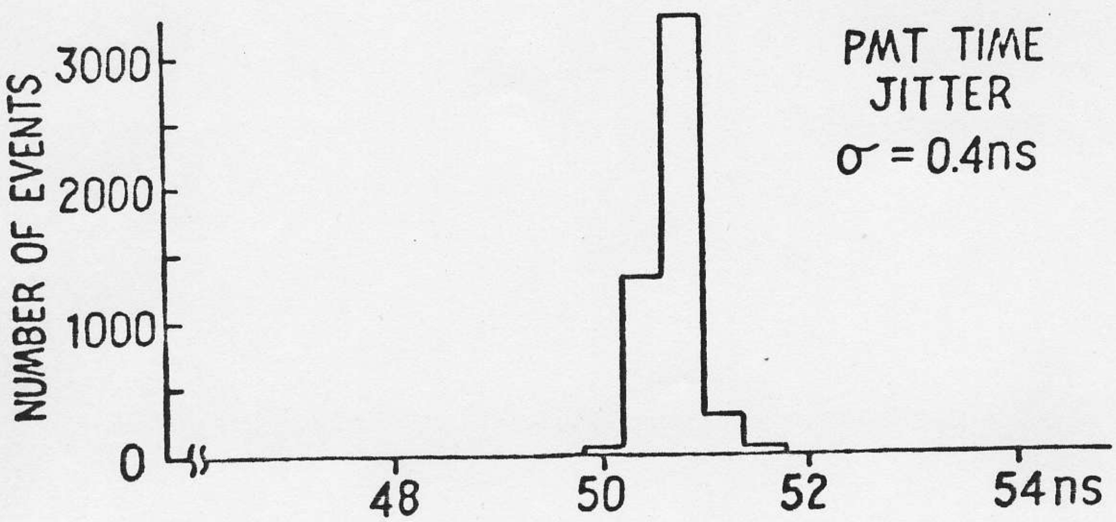

Figure 5. Photomultiplier Time Response

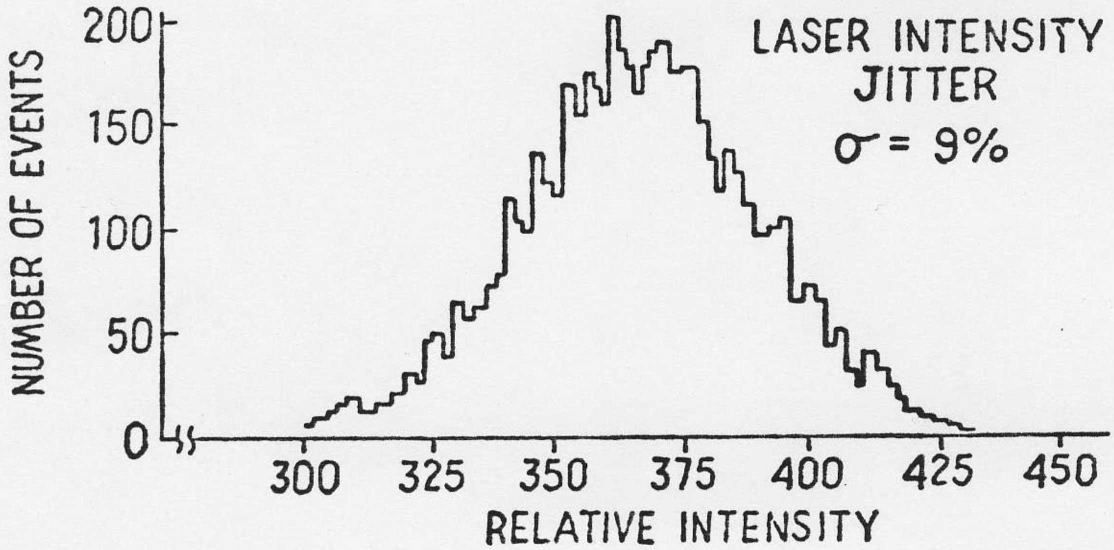

Figure 6. Laser Pulseheight Response

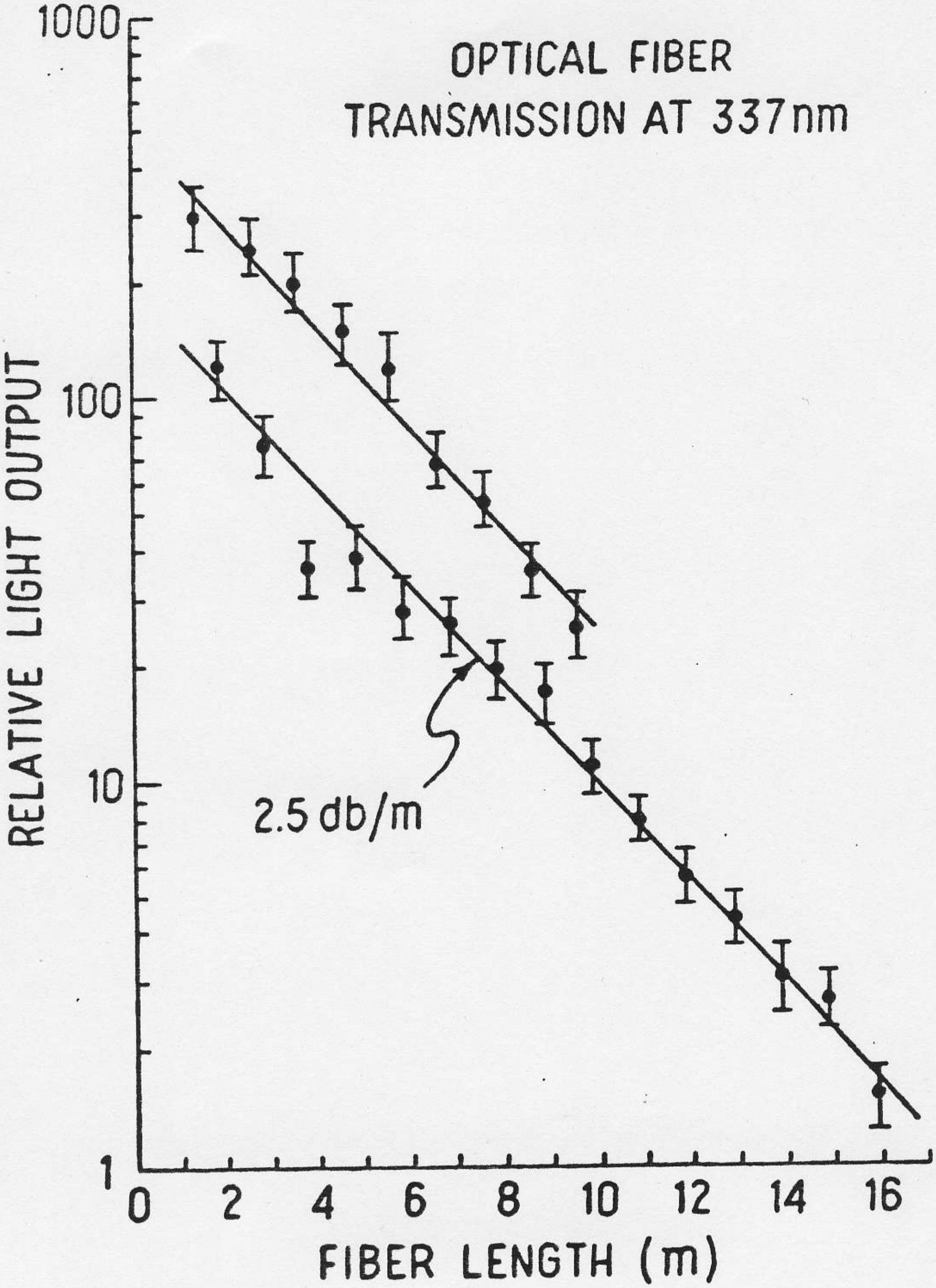

Figure 7. Optical Fiber Transmission at 337 nm

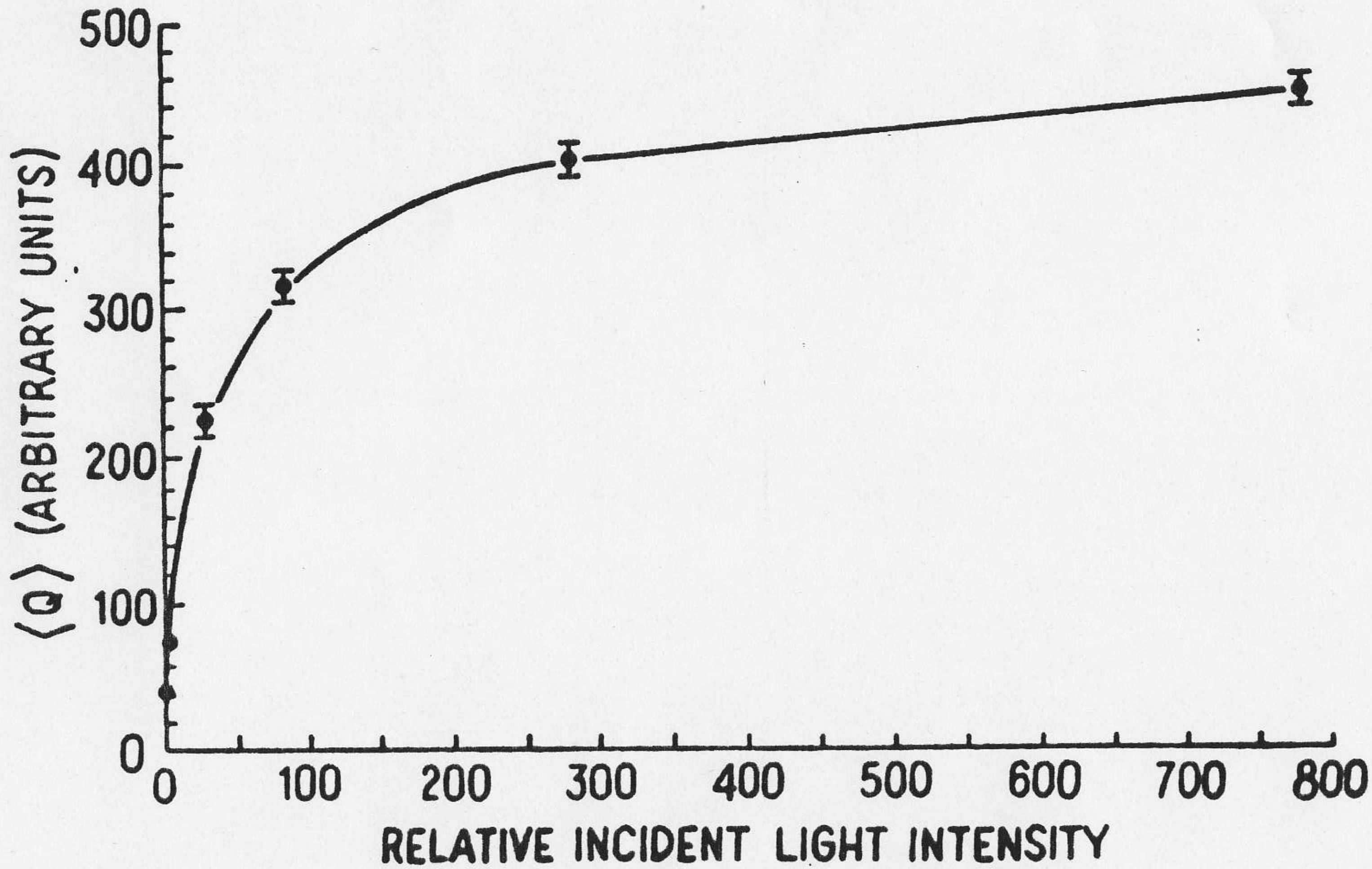

Figure 9. Average PMT Charge Output vs. Relative Light Insensity

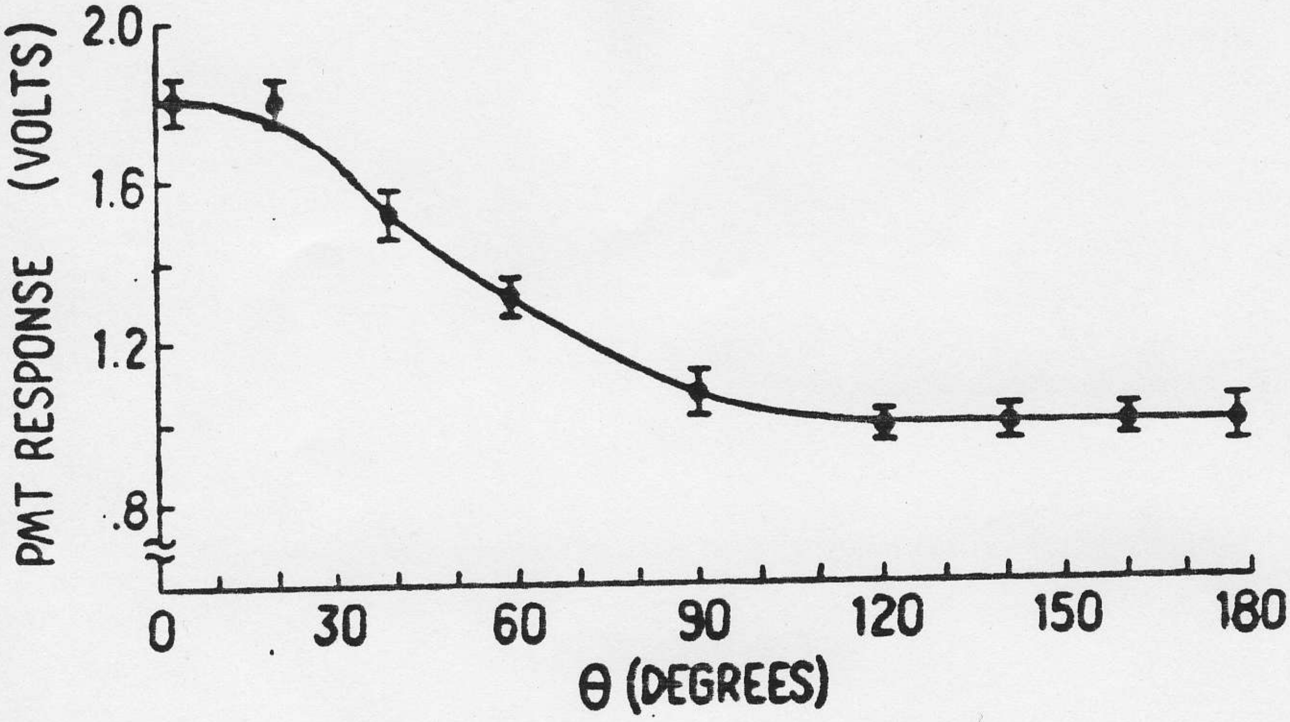

Figure 8a. Diffuser Light Intensity vs. Angle

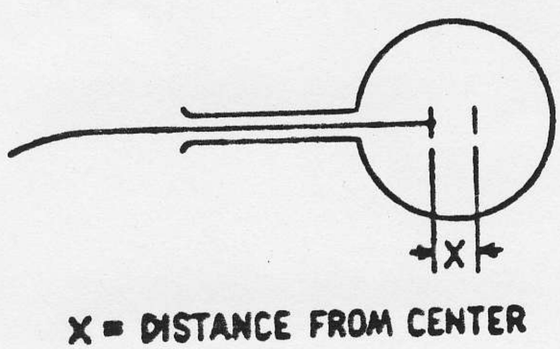

Figure 8b. Fiber End Placement in Diffuser